Extending the traveling range with a cascade electrostatic comb-drive actuator

2008 J. Micromech. Microeng. 18 015018

(http://iopscience.iop.org/0960-1317/18/1/015018)

J. Micromech. Microeng. **18** (2008) 015018 (7pp) doi:10.1088/0960-1317/18/1/015018

Extending the traveling range with a cascade electrostatic comb-drive actuator

Jin-Chern Chiou, Yung-Jiun Lin and Chin-Fu Kuo

Department of Electrical and Control Engineering, National Chiao Tung University, Hsin-Chu, Taiwan, Republic of China

E-mail: chiou@cc.nctu.edu.tw, yjlin@mail.nctu.edu.tw, chinfu_kuo@mail2000.com.tw

Received 20 April 2007, in final form 19 October 2007
Published 3 December 2007
Online at stacks.iop.org/JMM/18/015018

Abstract

Electrostatic comb-drive actuators have been developed and employed for many applications. However, side stability (side pull-in) limits the actuator stroke constraining its applications. Hence, extending the stable traveling range is an important issue for designing electrostatic comb-drive actuators. This study presents a novel cascade electrostatic comb-drive actuator. Instead of shifting the spring constant of the suspended springs, the proposed actuator extends the stable traveling range using a multi-stage cascade configuration. To demonstrate the performance of the cascade configuration, simulation using the finite element method is utilized to model the proposed cascade actuator. To implement the cascade electrostatic comb-drive actuator, the Taiwan Semiconductor Manufacturing Company (TSMC) 0.35 μm two-polysilicon and four-metal layer (2p4m) CMOS processes and post-CMOS micromachining steps are employed to fabricate the device. Experimental results demonstrate that the proposed design extends the stable traveling range to 200% as compared with that of a comb-drive actuator without this cascade configuration.

(Some figures in this article are in colour only in the electronic version)

1. Introduction

Micro-electro-mechanical systems (MEMS) enable suspended microstructures to be moved precisely and integrated with microelectronic circuits monolithically on a chip to perform or provide analog tuning or digital switching of linear or angular motion [1]. Various MEMS-based actuators, such as thermal/bimetallic bimorph actuators [1–3], electromagnetic actuators [4, 5], piezoelectric actuators [6, 7] and electrostatic actuators [8, 9], have been developed and applied in various fields.

In most applications, electrostatic actuators are preferred due to their low power consumption and fast response. The simplest electrostatic actuator is a parallel-plate electrostatic actuator. Such actuators have been utilized in many applications such as accelerometers[1] [10, 11], deformable optics [12] and relays [13]. However, parallel-plate electrostatic actuators suffer from the pull-in phenomenon, which greatly constrains the stable traveling range of actuators (usually one-third of initial gap). To avoid the pull-in phenomenon, electrostatic comb-drive actuators have been developed [14]. This actuator consists of two interdigitated finger structures with one fixed and the other connected to suspended springs, as shown in figure 1(*a*). By applying a driving voltage between the movable comb fingers and fixed comb fingers, a displacement of movable comb fingers toward fixed comb fingers is generated by the attractive electrostatic force. An electrostatic comb-drive actuator offers a near constant force over a large range of displacements. This actuator becomes a preferred design for implementing the electrostatic actuator. Applications of electrostatic comb-drive actuators include resonators [15, 16], microgrippers [17], *x*–*y* microstages [18] and electromechanical filters [19].

Although electrostatic comb-drive actuators have these advantageous characteristics, the stable traveling range of the comb-drive actuator is limited by the electromechanical side instability (side pull-in). Side instability means the situations in which the movable comb fingers move perpendicular to the stroke direction and then make contact with the fixed comb fingers. As the overlapping comb fingers' area increases with the forward displacement of the actuator, the cross-axis force becomes larger and larger that causes the fingers to suddenly

[1] ADXL05 Accelerometer, Analog Devices Norwood, MA, USA.

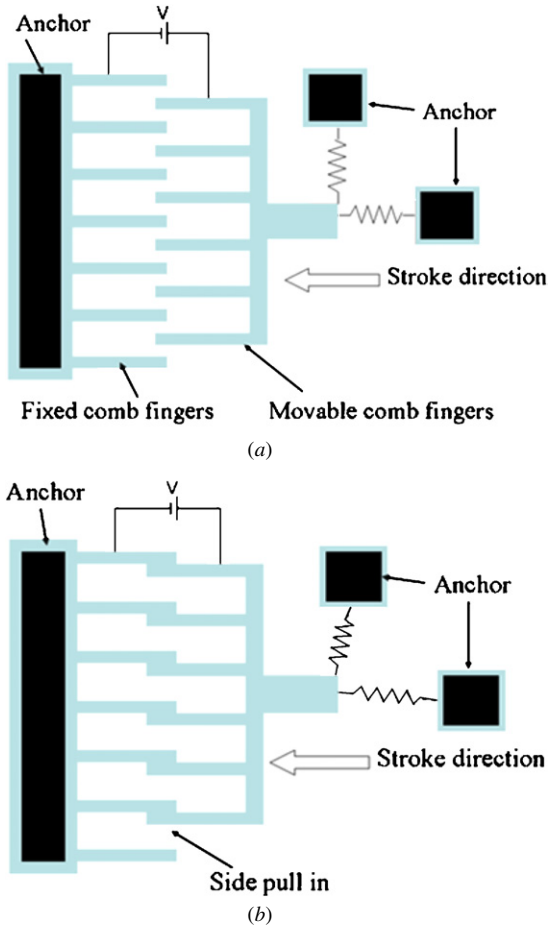

Figure 1. Schematic drawings of an electrostatic comb-drive actuator: (*a*) stable condition, (*b*) side instability condition.

snap over the sideway. Figure 1(*b*) shows the schematic diagram of the side instability condition. The side instability and stable traveling range of electrostatic comb-drive actuators depend on finger gap spacing, initial finger overlapping and spring stiffness of suspended springs. Increasing finger gap spacing of an electrostatic comb-drive actuator is the simplest method for increasing the stable traveling range; nevertheless, this method results in a high driving voltage which is undesirable in numerous applications.

To extend the stable traveling range of electrostatic comb-drive actuators, several approaches have been developed [20–23]. Among these methodologies, the most widely used method is to design different types of suspended springs to enhance the cross-axis stiffness which need extra driving voltage to extend the traveling range. Due to the fact, the present study proposes a novel cascade electrostatic comb-drive actuator that extends the stable traveling range through a novel cascade multi-stage configuration and does not require the addition of extra driving voltage. Furthermore, the proposed three cascade stages device can achieve a triple stroke as compared with the conventional electrostatic comb-drive actuator. With this in mind, this paper is organized as follows. In section 2, the electromechanical side instability of the electrostatic comb-drive actuator is characterized. The design of the cascade electrostatic comb-drive actuator along with simulation results and corresponding performance is given in section 3. In section 4, the Taiwan Semiconductor Manufacturing Company (TSMC) 0.35 μm two-polysilicon and four-metal layer (2p4m) CMOS processes and post-CMOS micromachining steps are described. Measurement results and conclusion are given in section 5 and section 6, respectively.

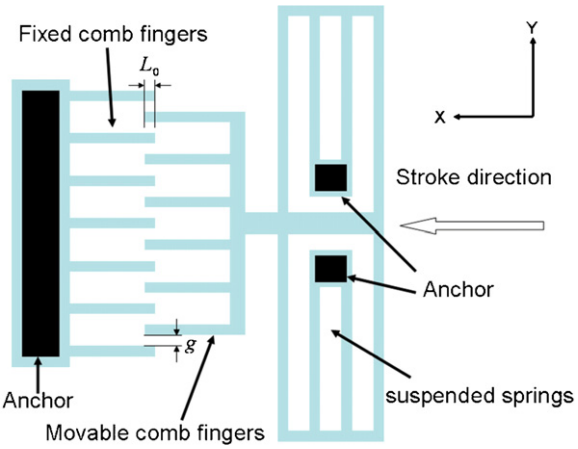

Figure 2. Schematic drawing of a conventional electrostatic comb-drive actuator.

2. Side instability

Figure 2 shows a conventional electrostatic comb-drive actuator. By applying a driving voltage between fixed comb fingers and movable comb fingers, the electrostatic force F_x along the x-direction is

$$F_x = \frac{N\varepsilon t}{2g}V^2, \tag{1}$$

Here, N is the number of finger pairs, ε is the dielectric constant in air, t is the finger thickness and g is the finger gap spacing. Ideally, the net electrostatic force F_y along the y-direction is zero. However, if the movable comb finger structure moves a small displacement toward the fixed comb finger structure along the y-direction, the net electrostatic force F_y is changed into

$$F_x = \frac{N\varepsilon t(L_0+\delta_x)}{2(g-y)^2}V^2 - \frac{N\varepsilon T(L_0+\delta_x)}{2(g+y)^2}V^2, \tag{2}$$

where L_0 is the initial overlap of the comb fingers and the δ_x is the displacement of the comb fingers in the x-direction, which is given by

$$\delta_x = \frac{N\varepsilon t}{2gK_x}V^2, \tag{3}$$

where K_x is the spring constant of the suspended springs in the x-direction. This electrostatic force F_y does not pull the movable comb finger structure back to the original position, but pushes the movable comb finger structure further close to the fixed comb finger structure. It looks as if there was a 'negative' spring and causes the actuator unstable. According to Hirano *et al* [24], the equivalent 'negative' spring constant is defined as

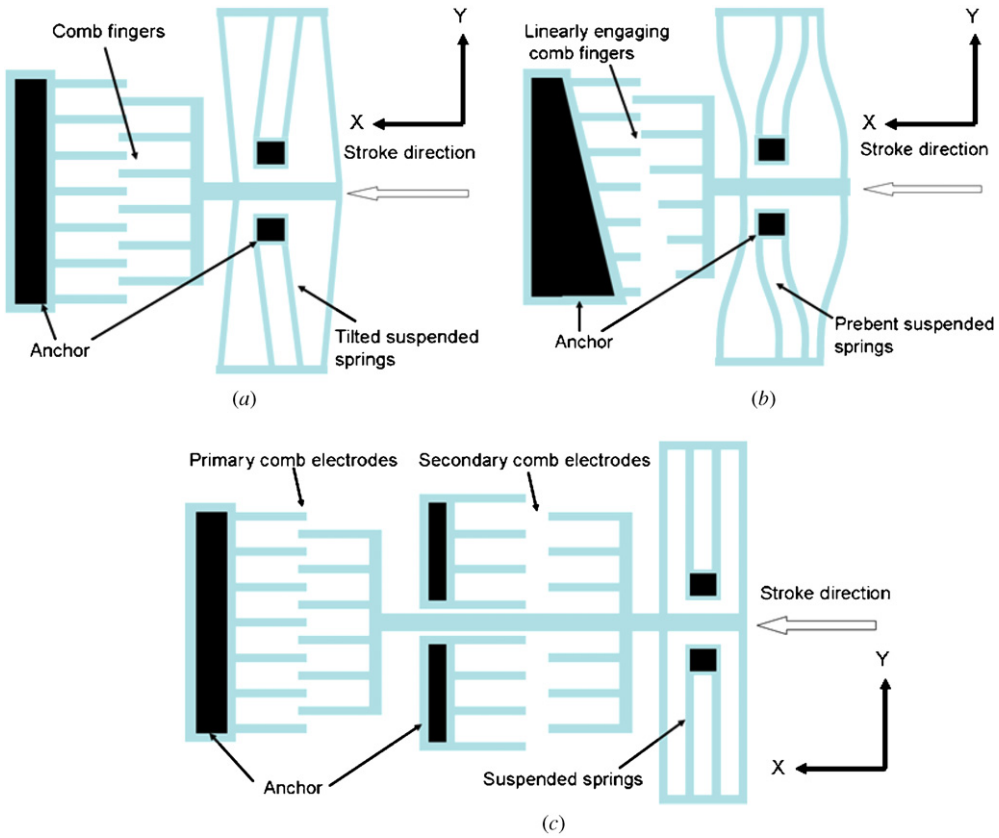

Figure 3. Schematic drawings of (*a*) an electrostatic comb-drive actuator with tilted suspended springs, (*b*) an electrostatic comb-drive actuator with pre-bent suspended springs and linearly engaging comb fingers, (*c*) an electrostatic comb-drive actuator with two sets of comb electrodes.

$$K_e = \left.\frac{\partial F_y}{\partial y}\right|_{y=0} = \frac{2N\varepsilon t(L_0+\delta_x)}{g^3}V^2. \tag{4}$$

The suspended springs could keep the moving comb finger structure against the instability of the electrostatic force. Hence, the stable condition of the comb-drive actuator is

$$K_y > \frac{2N\varepsilon t(L_0+\delta_x)}{g^3}V^2, \tag{5}$$

where K_y is the spring constant of the compliant suspension in the y-direction.

From equation (5), it is clear that increasing the finger gap spacing g increases the stable traveling range. However, increasing the finger gap spacing g reduces the electrostatic force in the x-direction that results in a higher driving voltage. Several approaches have been proposed to extend the stable traveling range [20–23]. Zhou and Dowd [20] used the tilted folded-beam suspended springs instead of the straight one to shift the spring constant in the y-direction. The corresponding spring constant in the y-direction changes from $\frac{200\,EI}{3\delta_x^2 l}$ to $\frac{600\,EI}{(3\delta_x-5d)^2 l}$, where E is Young's modulus, I is the inertia moment of the mechanical spring, d is the projection of the suspended beam length along the x-direction and l is the suspended beam length. Figure 3(*a*) shows the schematic drawing of the electrostatic comb-drive actuator with tilted fold-beam suspended springs. Another approach to extend the stable traveling range is to adjust the length of the individual comb fingers and utilize pre-bent suspended springs. Grade *et al* [21] demonstrated the comb-drive actuator with pre-bent suspended springs and linearly engaging comb fingers, as shown in figure 3(*b*). Recently, Hou *et al* [22] utilized the second comb electrode to extend the stable traveling range. This approach could shift K_e to extend the displacement of the electrostatic comb-drive actuator. Figure 3(*c*) shows the configuration of an electrostatic comb-drive actuator with two sets of comb electrodes. Although these approaches could extend the stable traveling range, they need extra driving voltage to extend the stable traveling range.

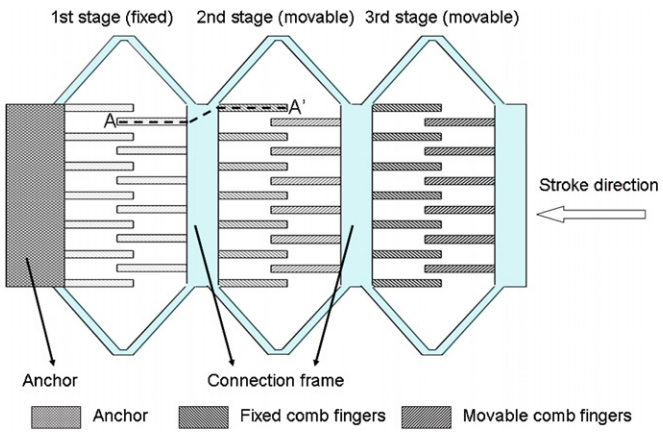

Figure 4. Schematic drawings of an electrostatic comb-drive actuator with three stages.

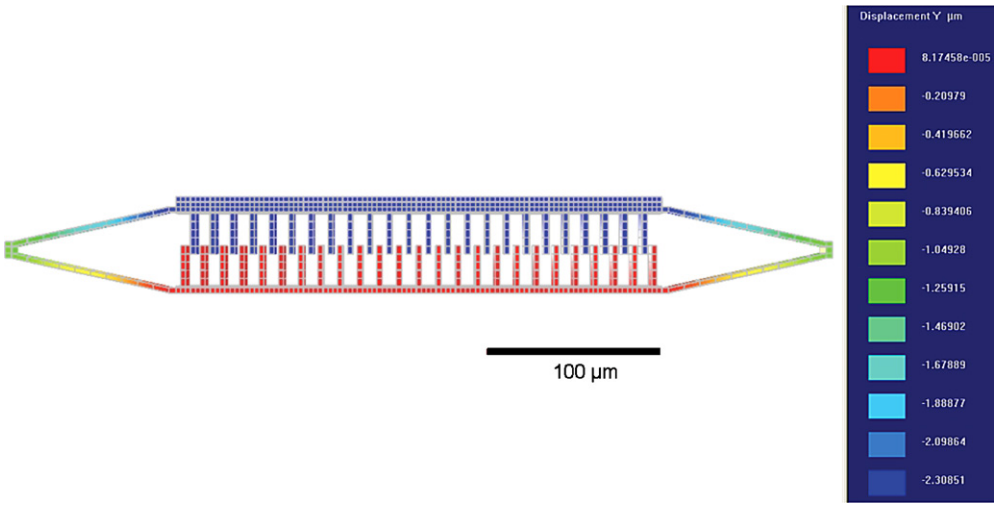

Figure 5. FEM simulation results of an electrostatic comb-drive actuator with 100 V driving voltage.

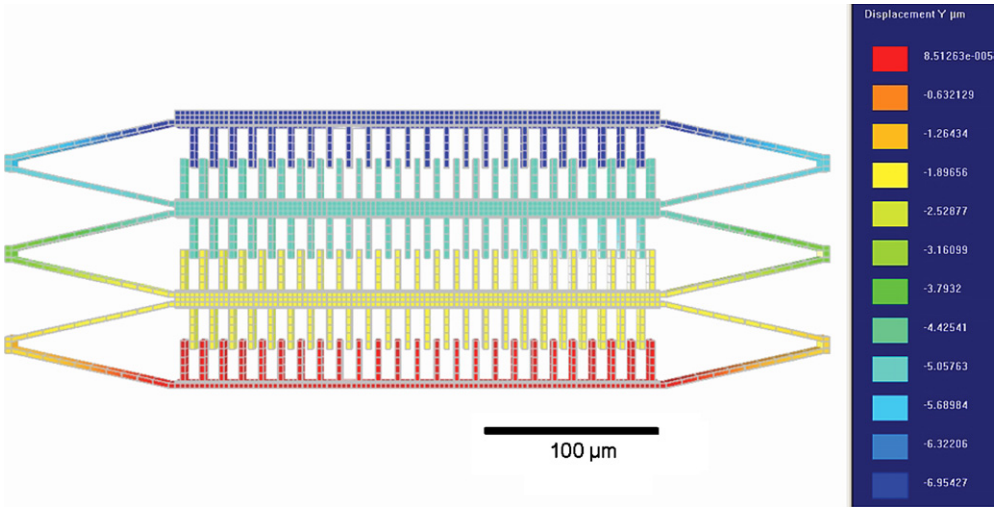

Figure 6. FEM simulation results of a cascade electrostatic comb-drive actuator with 100 V driving voltage.

3. Design concept

To extend the stable traveling range of the electrostatic comb-drive actuator without adding extra driving voltage, a novel electrostatic comb-drive actuator with a multi-stage cascade configuration is developed. Figure 4 shows schematic drawings of the cascade comb-drive actuator. This actuator comprises three stages, where the first stage is fixed and second and third stages are movable. Each stage contains a fixed comb finger structure, a movable comb finger structure and suspended springs. The neighboring two stages are linked by the connection frame. This indicates that the movable comb finger structure of one stage is connected with the fixed comb finger structure of the next stage. Consequently, all of the three stages are constructed with a multi-stage cascade configuration. Notably, each comb-drive actuator could be driven independently. By applying driving voltage to each stage, the stroke of the cascade actuator is the summation strokes of the first, second and third stages. Thus, the proposed cascade configuration actuator is capable of producing a stable extended traveling range.

In order to verify the performance of the proposed multi-stage cascade configuration, a finite element method (FEM) simulator, IntelliSuite®, is employed to model the actuator. Figure 5 shows the simulation result of an electrostatic comb-drive actuator with a single stage. The simulation result indicates that the stroke of the actuator is 2.3 μm with 100 V driving voltage. As shown in figure 6, by applying 100 V driving voltage to each of the multi-stage cascade electrostatic comb-drive actuator, a displacement of 6.9 μm is obtained. The simulation results indicated that the actuator with three cascade stages extends the stroke three times as compared with an actuator with only one single stage.

4. Fabrication process

To fabricate the cascade electrostatic comb-drive actuator, TSMC 0.35 μm 2p4m CMOS processes and post-CMOS micromachining steps are used. The CMOS processes consist of two polysilicon layers, four metal layers, three via layers and several dielectric layers/sacrificial layers. The four metal

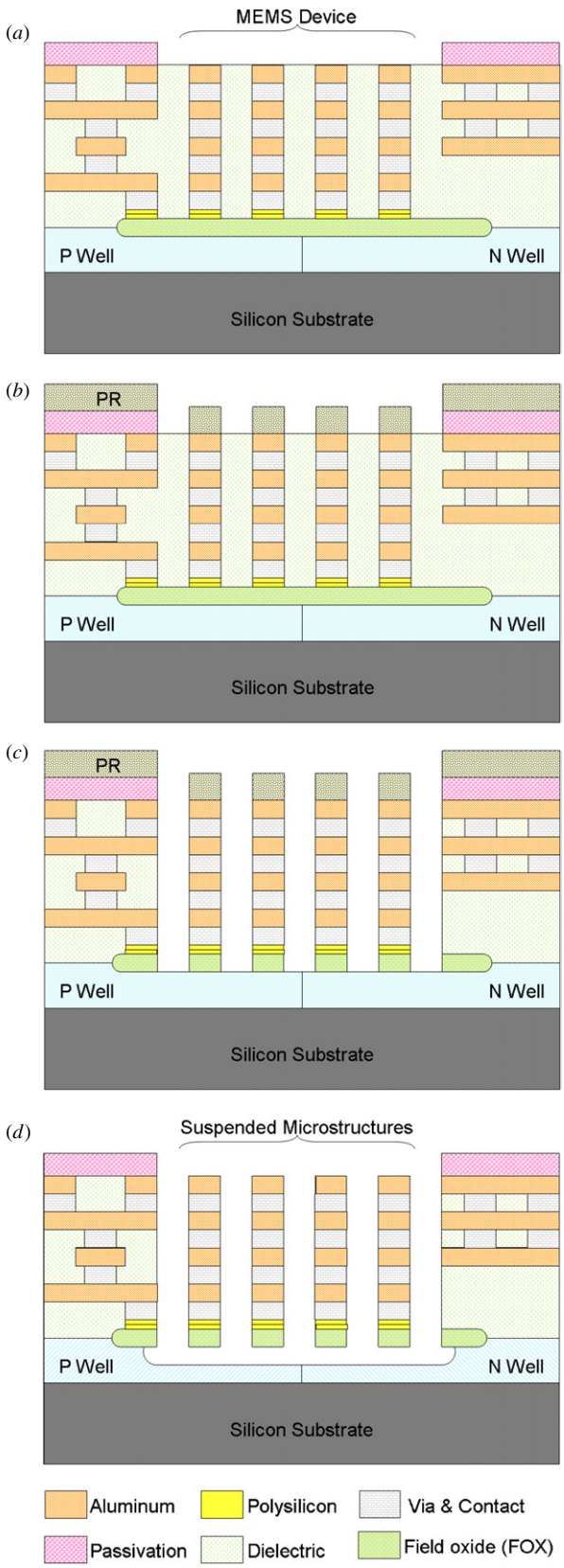

Figure 7. Post-CMOS micromachining steps: (*a*) cross-sectional view of MEMS devices after completing TSMC 0.35 2p4m fabrication processes, (*b*) patterning a PR mask to protect unneeded etched regions, (*c*) performing anisotropic RIE to etch silicon dioxide, (*d*) cross-sectional view of the device after completing the post-CMOS micromachining steps.

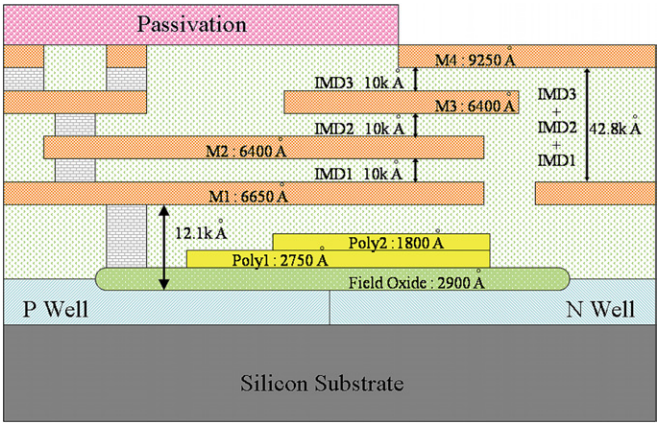

Figure 8. Thickness of each layer.

layers are made of aluminum. The contact and via holes are filled with tungsten plugs, and the dielectric layers/IMD (inter-metal dielectric) layers are made of silicon dioxide. The FOX (field oxide) layer is silicon dioxide. The etched holes are filled with silicon dioxide. In order to make the plane surface flat, chemical and mechanical polishing (CMP) is employed after each layer is completed. Figure 7(*a*) schematically depicts the cross-sectional view of the MEMS components fabricated through the TSMC 0.35 μm 2p4m CMOS process. Afterward, post-CMOS micromachining steps are performed to release the suspended structures of MEMS devices by etching the silicon dioxide and silicon substrate. The release steps need an additional photomask to define the etching areas. First, a thick photo-resist (PR) layer is coated on the chip and patterned as illustrated in figure 7(*b*). This patterned PR mask is used to protect the bonding pads, electronic circuit and the unneeded etched regions of the MEMS components during reactive-iron etch (RIE) processes. Then, an anisotropic RIE with a CHF3/O2 plasma is used to define the sidewalls of the device structure and etch the silicon dioxide in the etching holes. Figure 7(*c*) schematically shows the cross-sectional view of the MEMS device after anisotropic RIE processes. Next, an isotropic RIE with SF6/O2 is performed to etch the silicon underneath and release the suspended structures of the MEMS components. Finally, the PR layer is removed and completes the post-CMOS micromachining steps. Figure 7(*d*) schematically depicts the cross-sectional view of MEMS devices with released suspended structures after the post-CMOS micromachining steps. The thickness of each layer is given in figure 8.

As shown in figure 7, the device fabricated by the CMOS process consisted of several metal layers and dielectric layers. By performing post-CMOS micromachining steps, we are able to release a designed MEMS structure. With multilayer structures, every part of the device can be connected electrically via the metal layers. As shown in figure 9, the fixed comb finger structure and movable comb finger structure are connected by the connection frame; however, the fixed comb finger structure and movable comb finger structure are electrically isolated by the dielectric layers. Hence, each stage of the cascade structure can be driven

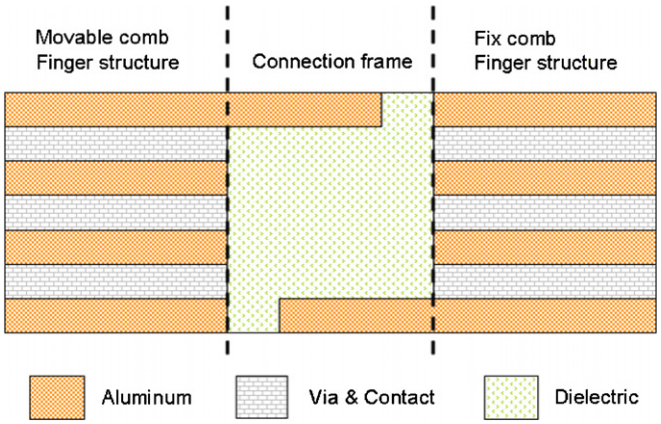

Figure 9. Schematic cross-sectional view of figure 4 at A–A′.

independently. To enhance the breakdown strength of the dielectric layer between the signal lines, M1 and M4 are employed as the actuation signal line; thus, a stacking dielectric layer, IMD1+IMD2+IMD3, design is utilized to increase the isolation thickness and raise the breakdown voltage between M1 and M4. As shown in figure 8, the thickness of IMD1+IMD2+IMD3 is 42.8 kÅ. Experimental results indicate that the stacking dielectric layer between M1 and M4 suffered no breakdown even with 200 V driving voltage. Notably, the structural part of the device is a composite. The material properties of each layer used in the simulation procedure are based on the material database of the MEMS simulator, IntelliSuite®.

5. Experimental results

Figure 10 shows the scanning electron microscopy (SEM) image of the fabricated device. The proposed cascade electrostatic comb-drive actuator consists of three stages. Each stage comprises 24 movable comb fingers and 25 fixed comb fingers. The length and width of a comb finger are 25 μm and 3 μm, respectively. The finger gap spacing and the initial finger overlap are both 3 μm. The size of the connection frame is 297 $\times$ 12 μm^2.

By applying driving voltage between movable comb fingers and fixed comb fingers, we are able to measure the performance of the fabricated device by using an optical interferometric profiler (WYKO). Figure 11 shows the static characteristic of the fabricated device by driving each stage independently. The critical voltage for side pull-in is 125 V. Before side pull-in occurs, the maximum displacement of the first, second and third stages are 3.6 μm, 3.4 μm and 3.2 μm respectively. Since the dimension of each stage is designed to be the same, thus we are expecting that the static characteristics of each stage should be the same. However, the measured static results of these three stages are different. It is due to the fact that the residual stress of the released device structure produced an out-of-plane bending as shown in figure 10(*b*). Figure 12 shows the displacement versus the dc driving voltage of the fabricated device by driving three stages simultaneously. With 125 V driving voltage, the overall displacement of the actuator is 10.1 μm.

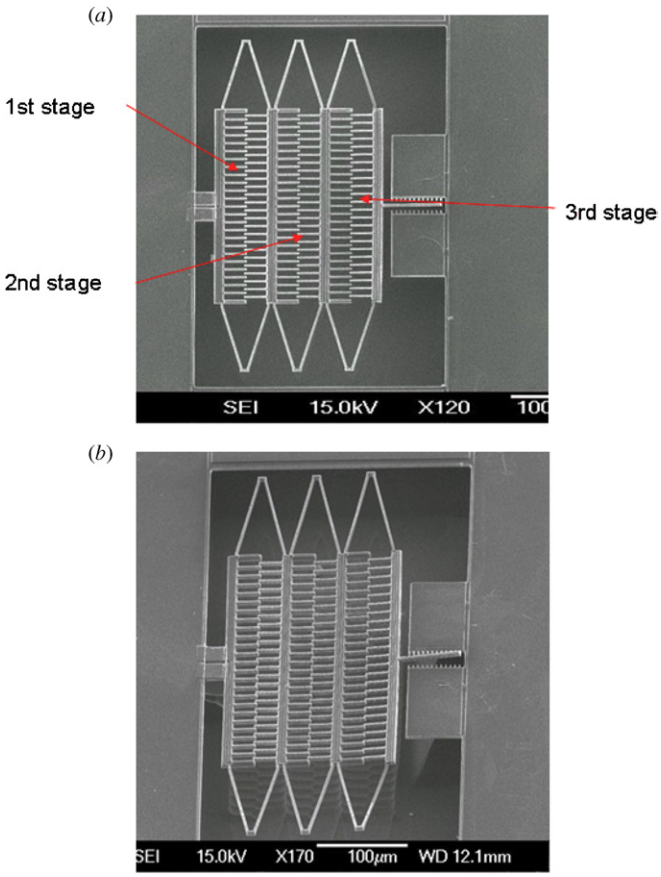

Figure 10. The SEM image of the fabricated device: (*a*) top view, (*b*) 45view.

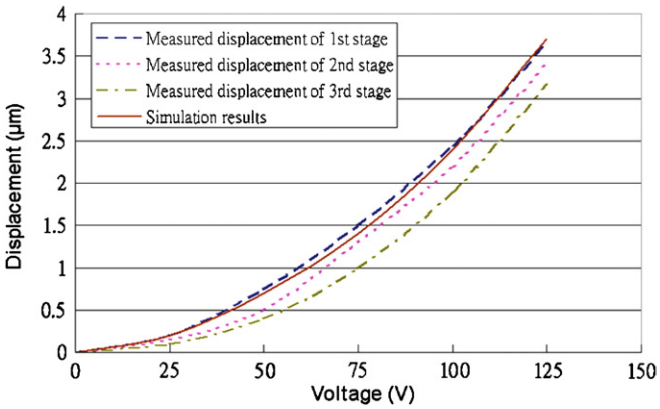

Figure 11. The static characteristic of the design cascade electrostatic comb-drive actuator device. The solid line represents the simulation results of the first stage and the dashed lines represent measured data of three different stages.

By comparing our experimental results with other approaches, the cascade structure can successfully extend the traveling range to nearly 200% without the need of extra driving voltage. Note that the approaches using the tilted folded-beam suspension [20] and secondary comb electrodes [22] can extend the traveling range up to 85% and 36%, respectively. This experimental result indicated that the design of the cascade structures is superior to previous designs in extending the traveling range.

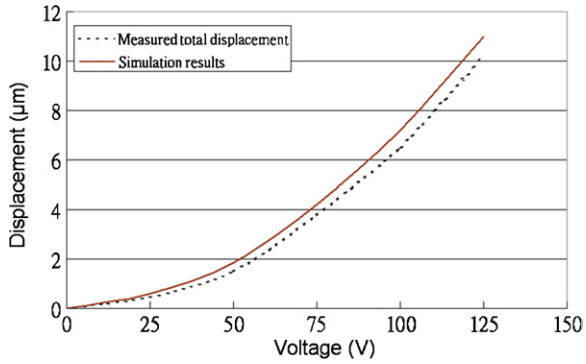

Figure 12. The displacement versus driving voltage by driving three stages simultaneously. The solid line corresponds to simulation results and the dotted line corresponds to measured data.

6. Conclusions

In this paper, a novel cascade electrostatic comb-drive actuator is proposed. The simulation results, the fabrication processes and the experimental results are given to verify the proposed device. With this novel cascade configuration, the stable traveling range is extended successfully. Measurement results indicated that the proposed cascade actuator extends the stroke nearly to 200% as compared with the actuator with a single stage. This cascade electrostatic comb-drive actuator will benefit the microsystems that require a large traveling stroke such as micro-*x*–*y* stages and variable optical attenuators.

Acknowledgments

This work was supported partly by the Ministry of Economic Affairs, Taiwan, Republic of China under contract no. NSC 95-EC-17-A-07-S1-011, the National Science Council, Taiwan, Republic of China under contract nos. NSC 95-2221-E-009-331 and NSC 95-2218-E009-017. The authors would also like to thank the National Chip Implementation Center (CIC) for their fabrication service.

References

[1] Mohamed A, Elsimar H and Ismail M 2003 Analysis, and optimization of a CMOS vertical thermal actuator *Proc. Symp. Design, Test, Integration and Packaging of MEMS/MOEMS* pp 214–7

[2] Popa D O, Byoung H K, Wen J T, Stephanou H E, Skidmore G and Geisberger A 2003 Dynamic modeling and input shaping of thermal bimorph MEMS actuators *Proc. IEEE Int. Conf. Robot. Autom.* vol 1 pp 1470–5

[3] Tuantranont A and Bright V M 2002 Micromachined thermal multimorph actuators fabricated by multi-users MEMS process *Proc. IEEE Int. Conf. Ind. Technol. (IEEE ICIT '02)* vol 2 pp 941–4

[4] Chowdhury S, Ahmadi M, Jullien G A and Miller W C 2000 A modular MEMS electromagnetic actuator for use in a hearing instrument *Proc. 43rd IEEE Midwest Symp. Circuits Syst.* vol 1 pp 240–3

[5] Ji C H, Kim Y K and Choi B K 2000 Design and fabrication of electromagnetic micromirror with bulk silicon mirror plate and aluminum spring *Proc. IEEE/LEOS Optical MEMS* pp 97–8

[6] Park J Y, Yee Y J, Nam H J and Bu J U 2001 Micromachined RF MEMS tunable capacitors using piezoelectric actuators *Proc. IEEE Microw. Symp. Dig.* vol 3 pp 2111–4

[7] Haddab Y, Chaillet N and Bourjault A 2000 A microgripper using smart piezoelectric actuators *Proc. IEEE Int. Conf. Intelligent Robots Syst. (IEEE/R S J IROS* vol 1*)* pp 659–64

[8] Hung E S and Senturia S D 1999 Extending the travel range of analog-tuned electrostatic actuators *J. Microelectromech. Syst.* **8** 497–05

[9] Mu X H, Kahrizi M and Landsberger L 2003 Design and fabrication of out-of-plane electrostatic actuators for optical application *Proc. IEEE Canadian Conf. Electri. Comput. Eng. (IEEE CCECE* vol 1*)* pp 133–6

[10] Yeh C and Najafi K 1998 CMOS interface circuitry for a low-voltage micromachined tunneling accelerometer *J. Microelectromech. Syst.* **7** 6–15

[11] Liu C-H, Barzilzi A M, Reynolds J K, Partridge A, Kenny T W, Grade J D and Rockstad H K 1998 Characterization of a high-sensitivity micromachined tunneling accelerometer with micro-g resolution *J. Microelectromech. Syst.* **7** 235–44

[12] Vdovin G, Sarro P M and Middelhoek S 1999 Technology and applications of micromachined adaptive mirrors *J. Micromech. Microeng.* **9** 8–19

[13] Zavracky P M, McGruer N E, Morrison R H and Potter D 1999 Microswitches and microrelays with a view toward microwave applications *Int. J. RF Microw. Comput.-Aided Eng.* **9** 338–47

[14] Tang W, Nguyen T and Howe R 1989 Laterally driven polysilicon resonant microstructures *Sensors Actuators* A **20** 25–32

[15] Tang W C 1990 Electrostatic comb drive for resonant sensor and actuator application *PhD Dissertation* Department of Electrical Engineering and Computer Sciences University of California Berkeley, CA, USA

[16] Weigold J W and Pang S W 1998 Fabrication of thick Si resonators with a frontside-release etch-diffusion process *J. Microelectromech. Syst.* **7** 201–6

[17] Kim C J, Pisano A P, Muller R S and Lim M G 1990 Polysilicon microgrippers *Tech. Dig. IEEE Solid-State Sensor Actuator Workshop (Hilton Head Island, SC, 1990)* pp 48–51

[18] Kim C-H, Jeong H-M, Jeon J-U and Kim Y-K 2003 Silicon micro xy-stage with a large area shuttle and no-etching holes for SPM-based data storage *J. Microelectromech. Syst.* **12** 470–8

[19] Lin L, Howe R T and Pisano A P 1998 Microelectromechanical filters for signal processing *IEEE J. Microelectromech. Syst.* **7** 286–94

[20] Zhou G and Dowd P 2003 Tilted folded-beam suspension for extending the stable travel range of comb drive actuators *J. Micromech. Microeng.* **13** 178–83

[21] Grade J D, Jerman H and Kenny T W 2003 Design of large deflection electrostatic actuators *J. Microelectromech. Syst.* **12** 335–43

[22] Hou M T-K, Huang G K-W, Huang J-Y, Liao K-M, Chen R and Yeh J-L A 2006 Extending displacements of comb drive actuators by adding secondary comb electrodes *J. Micromech. Microeng.* **16** 684–91

[23] Chen C and Lee C 2004 Design and modeling for comb drive actuator with enlarged static displacement *Sensors Actuators* A **115** 530–9

[24] Hirano T, Furuhata T and Gabriel K J 1992 Design, fabrication, and operation of submicron gap comb drive microactuator *J. Microelectromech. Syst.* **1** 52–9